Supplementary Information

Non-resonant Mie scattering: Emergent optical properties of core-shell polymer nanowires

Tural Khudiyev[1], Ersin Huseyinoglu[1,2] & Mehmet Bayindir[1,2,3*]

[1]UNAM-National Nanotechnology Research Center, Bilkent University, 06800 Ankara, Turkey

[2]Institute of Materials Science and Nanotechnology, Bilkent University, 06800 Ankara, Turkey

[3]Department of Physics, Bilkent University, 06800 Ankara, Turkey

[*]E-mail: bayindir@nano.org.tr

Table of Contents

S1 NRM scattering in various geometries	**3**
S2 Coupling-free scattering	**4**
S3 Field profiles of coupled nanowires	**5**
S4 Ellipsometric measurements of optical constants	**6**
S5 Measurement setup for structural coloration	**7**
S6 Analytical solutions for scattering from a core-shell nanowire	**8**
S7 Comparison of analytical solutions with FDTD simulations	**12**
S8 Absorption enhancement profiles for TM and TE polarized light	**13**

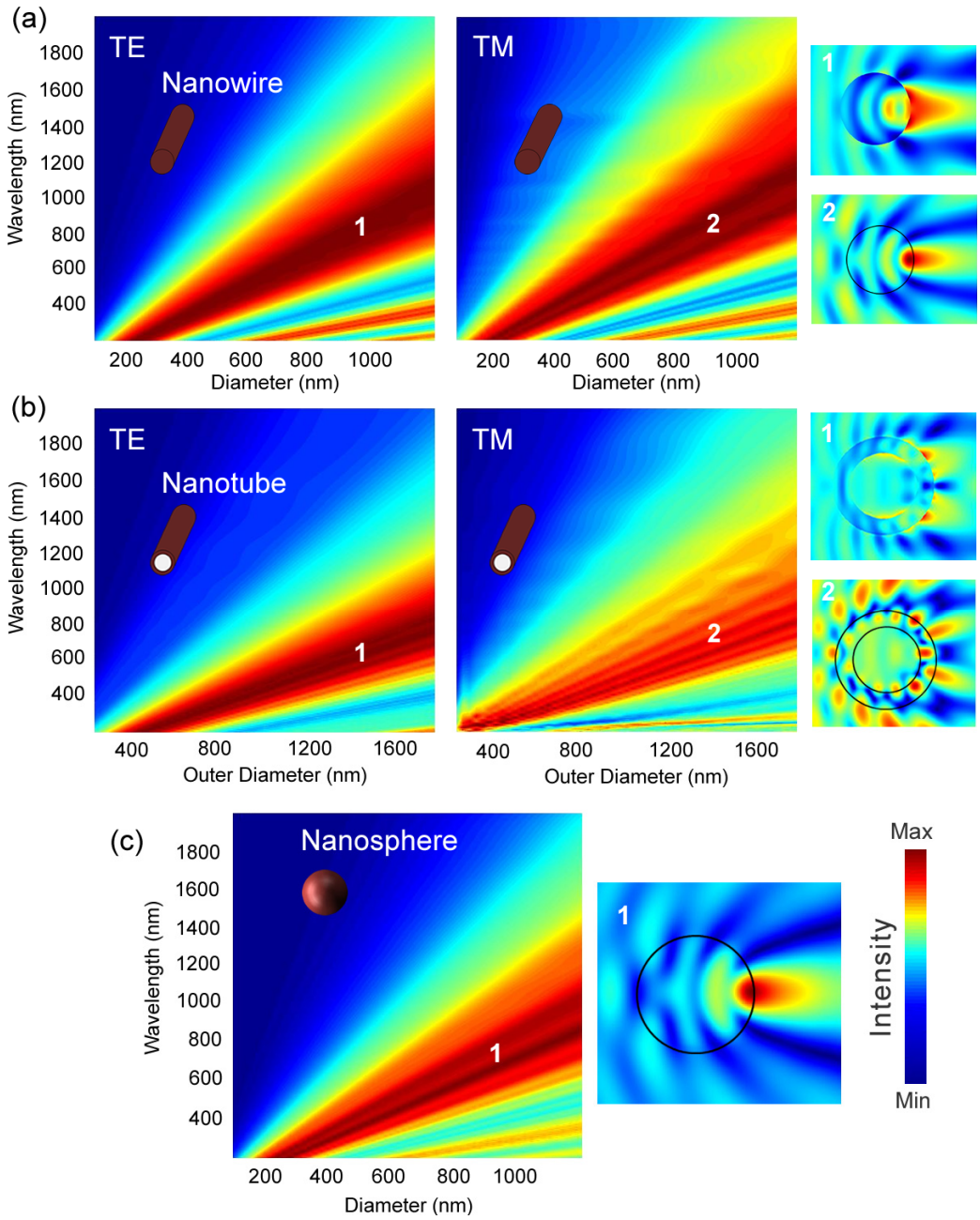

Figure S1 | NRM scattering in various geometries. (a) NRM scattering in bare nanowires. Electric field profiles of first order of TE and TM polarizations exhibit forward scattering behaviour, as would be expected. (b) Nanotube geometry is another interesting structure for the observation of this scattering regime. Field profiles of NRM scattering from this geometry differ from the nanowire case, although they also exhibit forward scattering behavior. Nanotubes are one of the most favorable geometries in microfluidics, therefore NRM scattering is also promising in this field. Inner/outer diameter ratio of the nanotube is 1:1.5 for all calculations. (c) For sphere geometry, non-resonant field distribution verifies forward-scattering feature as in 1D nanostructure cases.

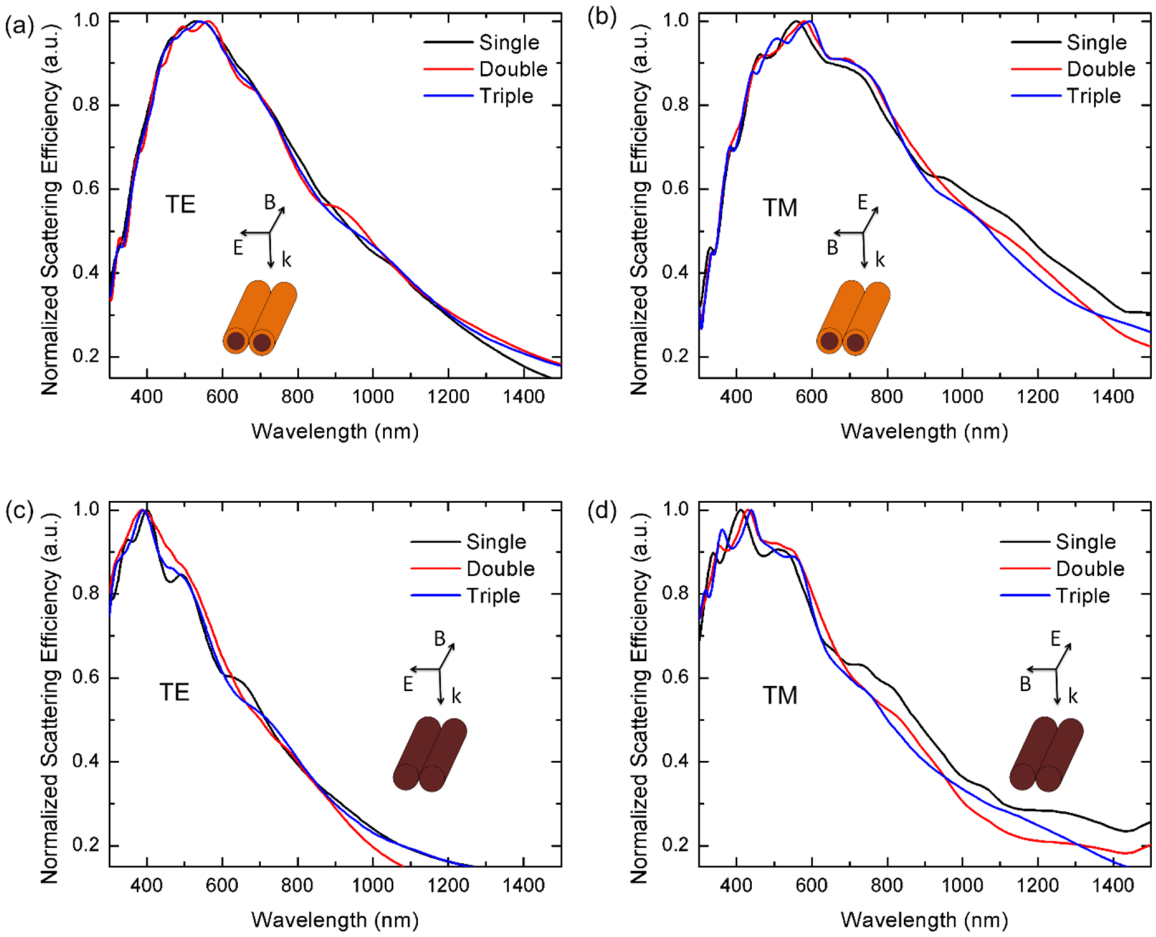

Figure S2 | Coupling-free scattering. Side-by-side nanowires (*i.e.* one, two and three coupled nanowires are shown as single, double and triple terms respectively in plots' inset) do not induce optical coupling, which is markedly different from resonant Mie scattering. For both (a) TE and (b) TM polarizations scattering spectrum is unaffected from number of side-by-side core-shell nanowires. (c,d) Same results hold for bare nanowires.

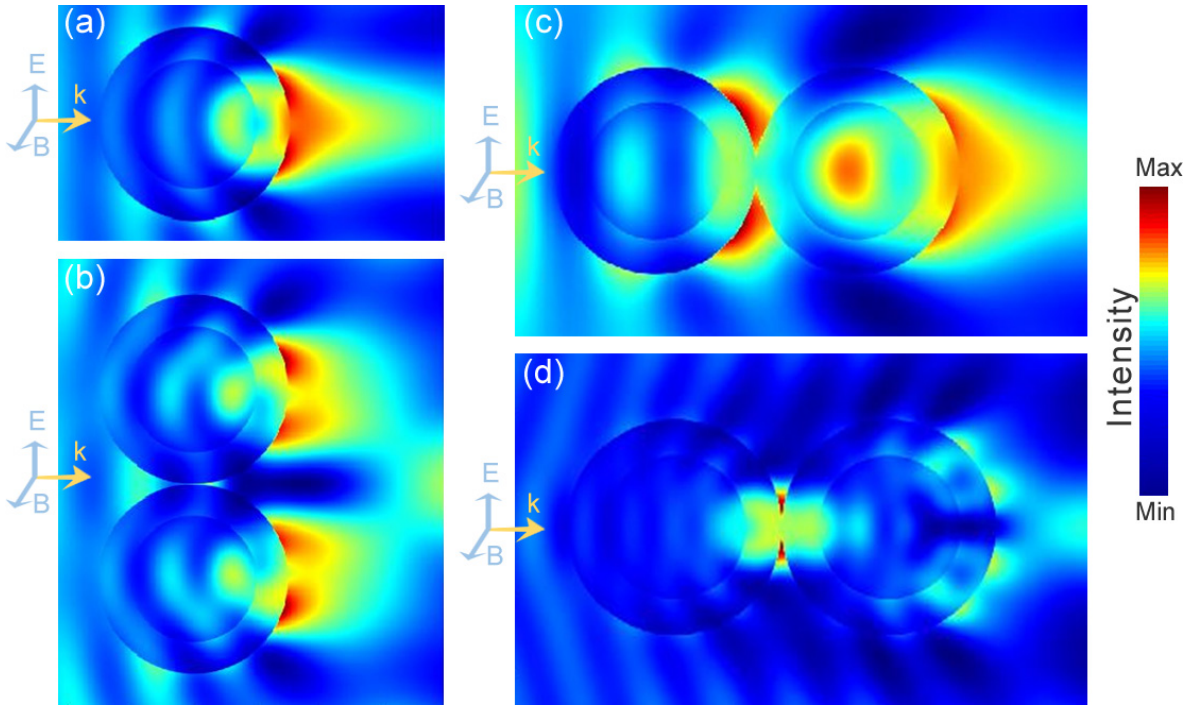

Figure S3 | Field profiles of coupled nanowires. (a**)** Near field profile of scattering from a single core-shell nanowire. (b) Field profile corresponds to a 550 nm peak in Figure 3a. Electric field distribution within the core-shell structure is almost unaffected from the number of nanowires that are arrayed side-by-side. (c-d) Scattered light exhibits coupled cavity behavior in overlapping nanowires. Profiles in (c) and (d) correspond to 1060 nm and 450 nm peaks in splitting, respectively shown in Figure 3b.

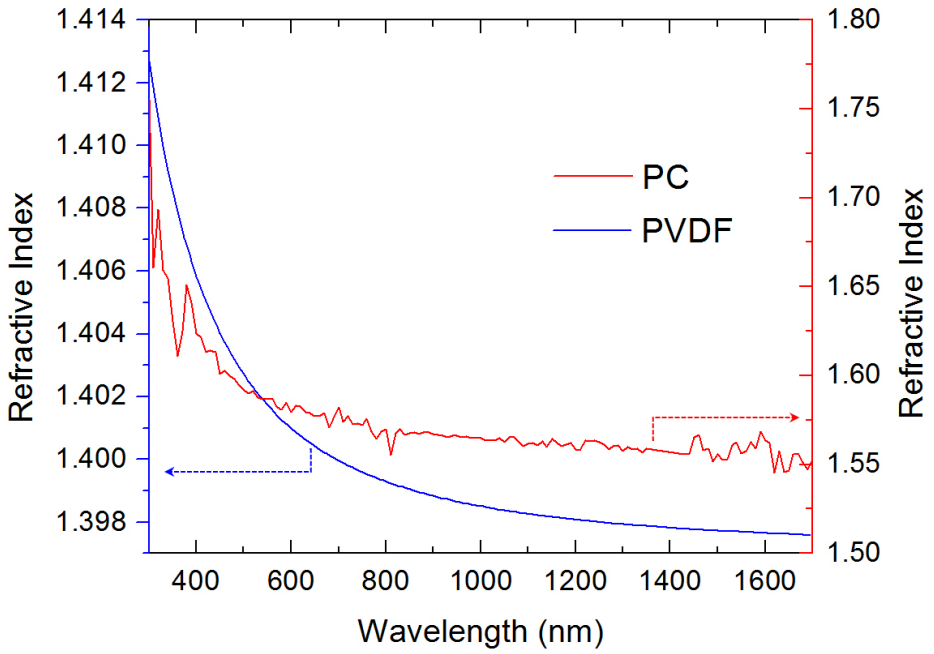

Figure S4 | Ellipsometric measurements of optical constants. Optical properties of used polymers, PVDF and PC, are investigated by spectroscopic ellipsometer. PC which is used as a core polymer possesses average refractive index of 1.58. On the other hand, PVDF which is used as a shell layer has lower, average optical index of 1.41. There is no significant absorption for both polymers in the visible spectrum.

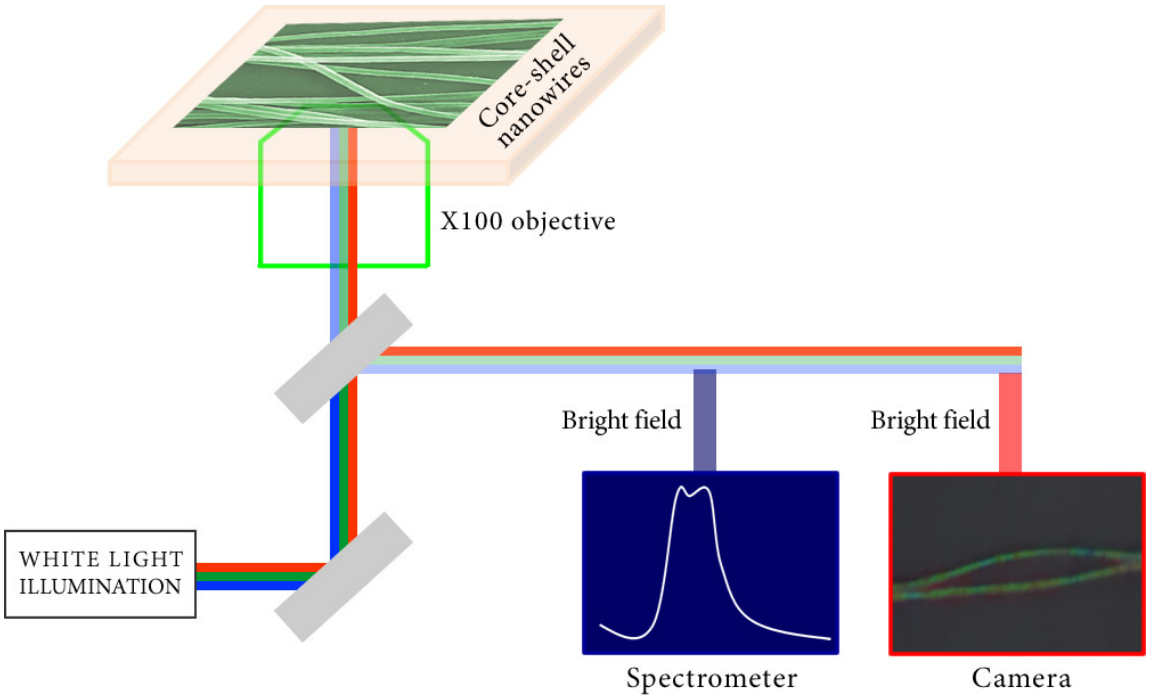

Figure S5 | Measurement setup for structural coloration. Schematics of experimental set-up used for scattering measurements of polymer nanowires. Optical microscope images of individual colored nanowires, are obtained in bright field mode of an inverted microscope. The scattered light is collected by a UV-Vis-NIR MAYA spectrometer coupled to the microscope.

Analytical Solution of Light Scattering from Core-Shell Nanostructures:

Lorenz-Mie Formalism

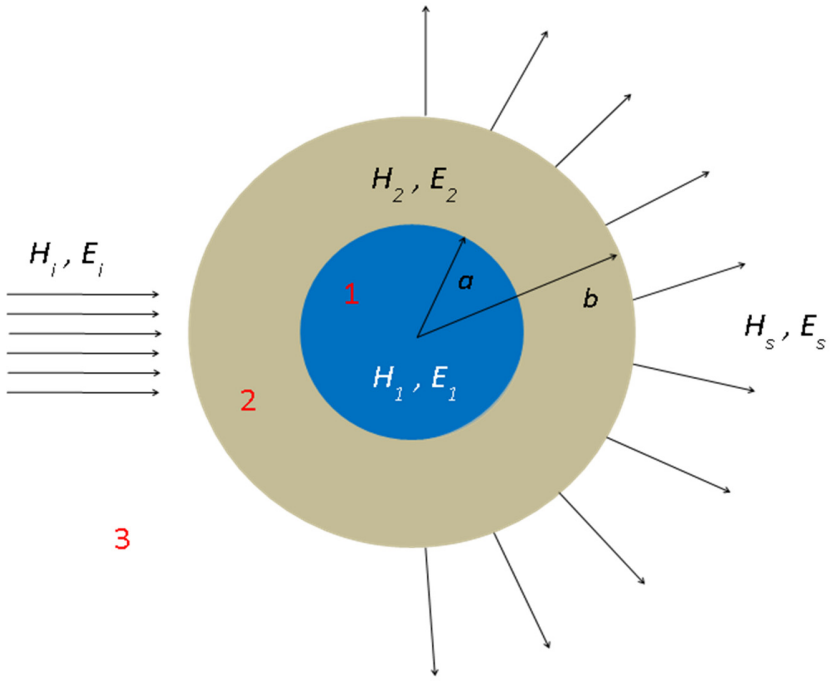

Figure S6 | Schematic of the analytical solutions for scattering from a core-shell nanowire. The core medium possesses a higher refractive index than the shell region in our core-shell nanowires. Subscripts i and s indicate incident and scattered fields, respectively.

Setup of equations (TM):

$$E_{\mathrm{i}} = \sum_{n=-\infty}^{\infty} E_n {N_n}^{(i)}$$

$$H_{\mathrm{i}} = \frac{-ik}{\omega\mu} \sum_{n=-\infty}^{\infty} E_n {M_n}^{(i)}$$

$$E_1 = \sum_{n=-\infty}^{\infty} E_n \left(c_n {M_n}^{(1)} + d_n {N_n}^{(1)}\right)$$

$$H_1 = \frac{-ik_1}{\omega\mu_1} \sum_{n=-\infty}^{\infty} E_n \left(c_n {N_n}^{(1)} + d_n {M_n}^{(1)}\right)$$

$$E_2 = \sum_{n=-\infty}^{\infty} E_n \left(g_n {M_n}^{(2j)} + f_n {N_n}^{(2j)} + v_n {M_n}^{(2y)} + w_n {N_n}^{(2y)}\right)$$

$$H_2 = \frac{-ik_2}{\omega\mu_2} \sum_{n=-\infty}^{\infty} E_n \left(f_n {M_n}^{(2j)} + \mathrm{g}{N_n}^{(2j)} + w_n {M_n}^{(2y)} + v_n {N_n}^{(2y)}\right)$$

$$E_{\mathrm{s}} = -\sum_{n=-\infty}^{\infty} E_n \left(b_{n1} {N_n}^{(3)} + i a_{n1} {M_n}^{(3)}\right)$$

$$H_{\mathrm{s}} = \frac{ik}{\omega\mu} \sum_{n=-\infty}^{\infty} E_n \left(b_{n1} {M_n}^{(3)} + i a_{n1} {N_n}^{(3)}\right)$$

Setup of equations (TE):

$$E_{\mathrm{i}} = -i \sum_{n=-\infty}^{\infty} E_n {M_n}^{(i)}$$

$$H_{\mathrm{i}} = \frac{-k}{\omega\mu} \sum_{n=-\infty}^{\infty} E_n {N_n}^{(i)}$$

$$E_1 = -i \sum_{n=-\infty}^{\infty} E_n \left(c_n {M_n}^{(1)} + d_n {N_n}^{(1)}\right)$$

$$H_1 = \frac{-k_1}{\omega\mu_1} \sum_{n=-\infty}^{\infty} E_n \left(c_n {N_n}^{(1)} + d_n {M_n}^{(1)}\right)$$

$$E_2 = -i\sum_{n=-\infty}^{\infty} E_n\left(g_n {M_n}^{(2j)} + f_n {N_n}^{(2j)} + v_n {M_n}^{(2y)} + w_n {N_n}^{(2y)}\right)$$

$$H_2 = \frac{-k_2}{\omega\mu_2}\sum_{n=-\infty}^{\infty} E_n\left(f_n {M_n}^{(2j)} + \mathrm{g}{N_n}^{(2j)} + w_n {M_n}^{(2y)} + v_n {N_n}^{(2y)}\right)$$

$$E_{\mathrm{s}} = \sum_{n=-\infty}^{\infty} E_n\left(b_{n2} {N_n}^{(3)} + i a_{n2} {M_n}^{(3)}\right)$$

$$H_{\mathrm{s}} = \frac{k}{\omega\mu}\sum_{n=-\infty}^{\infty} E_n\left(i b_{n2} {M_n}^{(3)} + a_{n2} {N_n}^{(3)}\right)$$

Boundary conditions:

$$(E_2 - E_1)\times\hat{r} = 0 \qquad (H_2 - H_1)\times\hat{r} = 0 \qquad @ \quad r = a$$

$$(E_s + E_i - E_2)\times\hat{r} = 0 \qquad (H_s + H_i - H_2)\times\hat{r} = 0 \qquad @ \quad r = b$$

Generating functions:

$$M_n = \nabla\times(\hat{z}\Psi_n)$$

$$N_n = \frac{\nabla\times(M_n)}{k}$$

$$M_n = \sqrt{k^2 - h^2}\left(in\frac{Z_n(\rho)}{\rho}\hat{r} - Z_n'(\rho)\hat{\varphi}\right)e^{i(n\varphi + hz)}$$

$$N_n = \frac{\sqrt{k^2 - h^2}}{k}\left(ihZ_n'(\rho)\hat{r} - hn\frac{Z_n(\rho)}{\rho}\hat{\varphi} + \sqrt{k^2 - h^2}Z_n(\rho)\hat{z}\right)e^{i(n\varphi + hz)}$$

$$h = -k\cos\gamma$$

$$\Psi_n^i = J_n(kr\sin\gamma)e^{i(n\varphi)}e^{-i(kz\cos\gamma)}$$

$$\Psi_n^s = H_n^{(1)}(kr\sin\gamma)e^{i(n\varphi)}e^{-i(kz\cos\gamma)}$$

$$\Psi_n^1 = J_n\left(kr\sqrt{m_1^2 - \cos^2\gamma}\right)e^{i(n\varphi)}e^{-i(kz\cos\gamma)}$$

$$\Psi_n^2 = \left(cJ_n\left(kr\sqrt{m_2^2 - \cos^2\gamma} + dY_n\left(kr\sqrt{m_2^2 - \cos^2\gamma}\right)\right)e^{in\varphi}e^{-i(kz\cos\gamma)}\right.$$

M wavevector	N wavevector
$M_n^i = ksin\gamma(in\frac{J_n(krsin\gamma)}{krsin\gamma}\hat{r} - J_n'(krsin\gamma)\hat{\varphi})e^{i(n\varphi - kzcos\gamma)}$	$N_n^i = sin\gamma(-ikcos\gamma J_n'(krsin\gamma)\hat{r} + kncos\gamma\frac{J_n(krsin\gamma)}{krsin\gamma}\hat{\varphi} + ksin\gamma J_n(krsin\gamma)\hat{z})e^{i(n\varphi - kzcos\gamma)}$
$M_n^3 = ksin\gamma(in\frac{H_n^{(1)}(krsin\gamma)}{krsin\gamma}\hat{r} - H_n'^{(1)}(krsin\gamma)\hat{\varphi})e^{i(n\varphi - kzcos\gamma)}$	$N_n^3 = sin\gamma\left(-ikcos\gamma H_n'^{(1)}(krsin\gamma)\hat{r} + kncos\gamma\frac{H_n^{(1)}(krsin\gamma)}{krsin\gamma}\hat{\varphi} + ksin\gamma H_n^{(1)}(krsin\gamma)\hat{z}\right)e^{i(n\varphi - kzcos\gamma)}$
$M_n^1 = k_1 sin\gamma(in\frac{J_n(kr\sqrt{m_1^2 - cos^2\gamma})}{k_1 rsin\gamma}\hat{r} - J_n'(kr\sqrt{m_1^2 - cos^2\gamma})\hat{\varphi})e^{i(n\varphi - kzcos\gamma)}$	$N_n^1 = sin\gamma\left(-ikcos\gamma J_n'(kr\sqrt{m_1^2 - cos^2\gamma})\hat{r} + k_1 ncos\gamma\frac{J_n(kr\sqrt{m_1^2 - cos^2\gamma})}{k_1 rsin\gamma}\hat{\varphi} + k_1 sin\gamma J_n(kr\sqrt{m_1^2 - cos^2\gamma})\hat{z}\right)e^{i(n\varphi - kzcos\gamma)}$
$M_n^{2j} = k_2 sin\gamma(in\frac{J_n(kr\sqrt{m_2^2 - cos^2\gamma})}{k_2 rsin\gamma}\hat{r} - J_n'(kr\sqrt{m_2^2 - cos^2\gamma})\hat{\varphi})e^{i(n\varphi - kzcos\gamma)}$	$N_n^{2j} = sin\gamma\left(-ik_2 cos\gamma J_n'(kr\sqrt{m_2^2 - cos^2\gamma})\hat{r} + k_2 ncos\gamma\frac{J_n(kr\sqrt{m_2^2 - cos^2\gamma})}{k_2 rsin\gamma}\hat{\varphi} + k_2 sin\gamma J_n(kr\sqrt{m_2^2 - cos^2\gamma})\hat{z}\right)e^{i(n\varphi - kzcos\gamma)}$
$M_n^{2y} = k_2 sin\gamma(in\frac{Y_n(kr\sqrt{m_2^2 - cos^2\gamma})}{k_2 rsin\gamma}\hat{r} - Y_n'(kr\sqrt{m_2^2 - cos^2\gamma})\hat{\varphi})e^{i(n\varphi - kzcos\gamma)}$	$N_n^{2y} = sin\gamma\left(-ik_2 cos\gamma Y_n'(kr\sqrt{m_2^2 - cos^2\gamma})\hat{r} + k_2 ncos\gamma\frac{Y_n(kr\sqrt{m_2^2 - cos^2\gamma})}{k_2 rsin\gamma}\hat{\varphi} + k_2 sin\gamma Y_n(kr\sqrt{m_2^2 - cos^2\gamma})\hat{z}\right)e^{i(n\varphi - kzcos\gamma)}$

Table S1 | Generating functions regarding to all three regions in the core-shell nanowire.

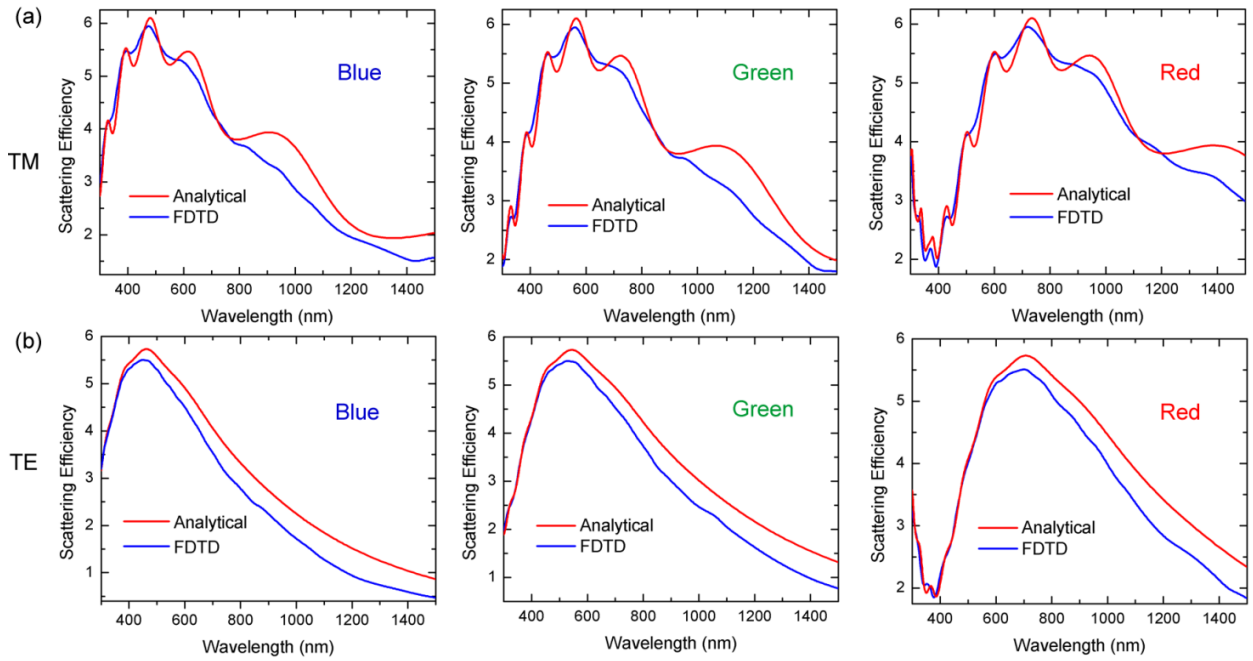

Figure S7 | Comparison of analytical solutions with FDTD simulations. Analytically solved scattering equations for both (a) TE and (b) TM polarizations is compared with FDTD simulation results. The method used for analytical solutions is based on vector wave harmonic expansion of scattered light. Simulated results are in good agreement with theoretical calculations. Nanowires used for comparison have core diameters of 340, 400, 520 nm for blue, green, and red coloration, respectively.

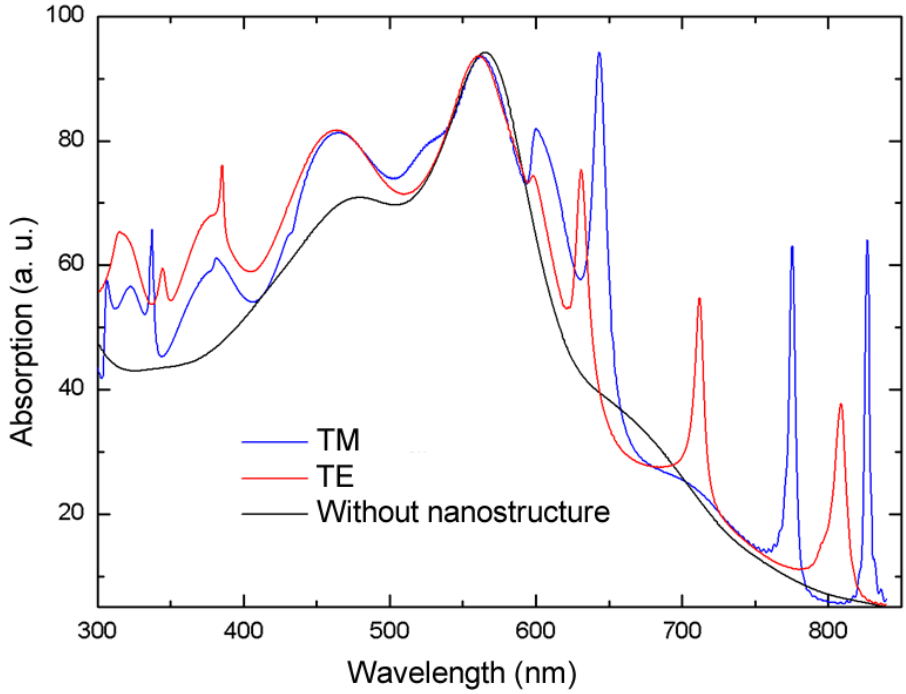

Figure S8 | Absorption enhancement profiles for TM and TE polarized light. Both in TE and TM polarization of light, NRM scattering induces light accumulation inside of thin film solar cells and results with similar enhancement profiles and rates. Calculated enhancement values (compared to bare thin film solar cell) are 14.5% for TE and 14.6% for TM polarization case.